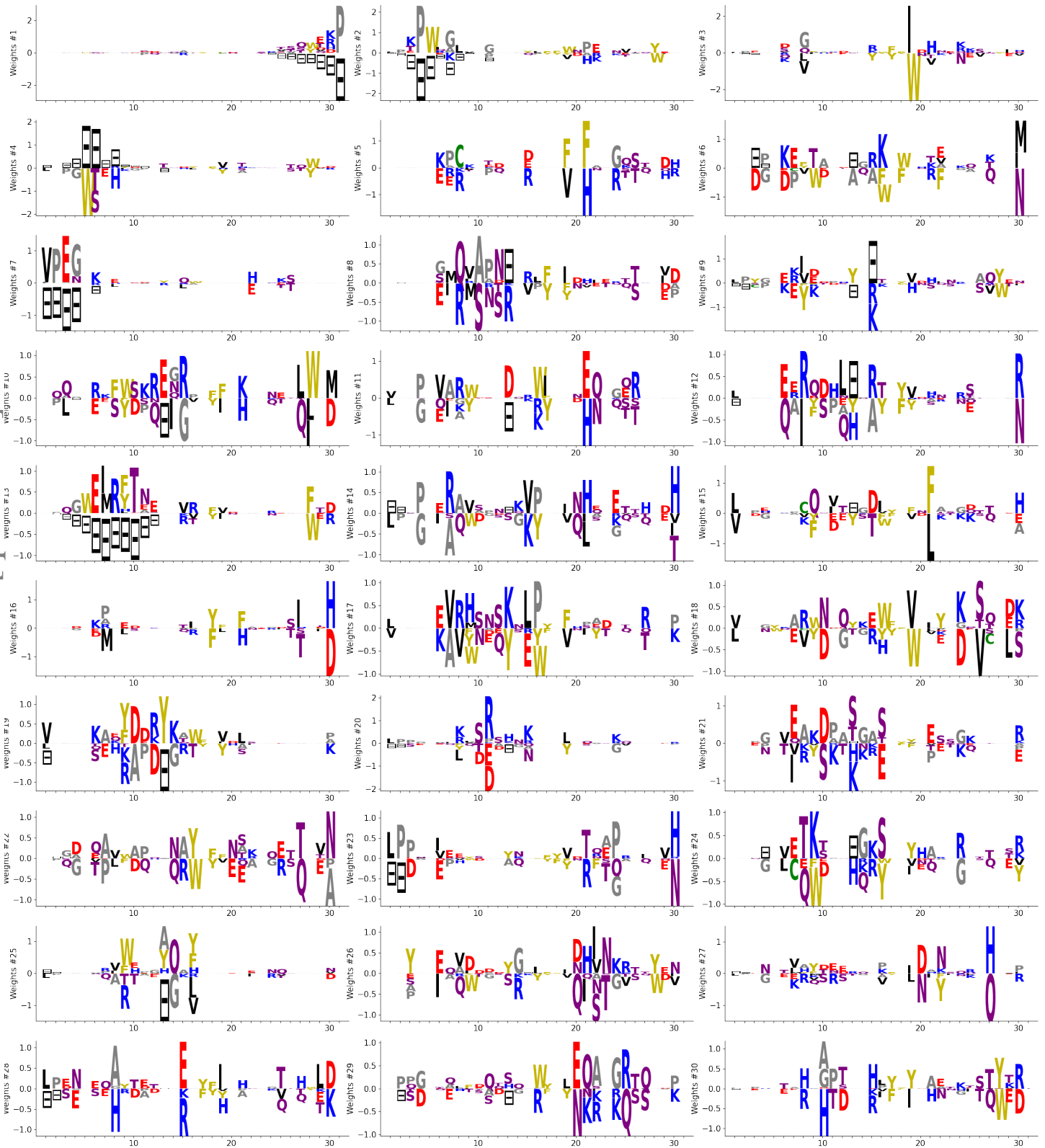
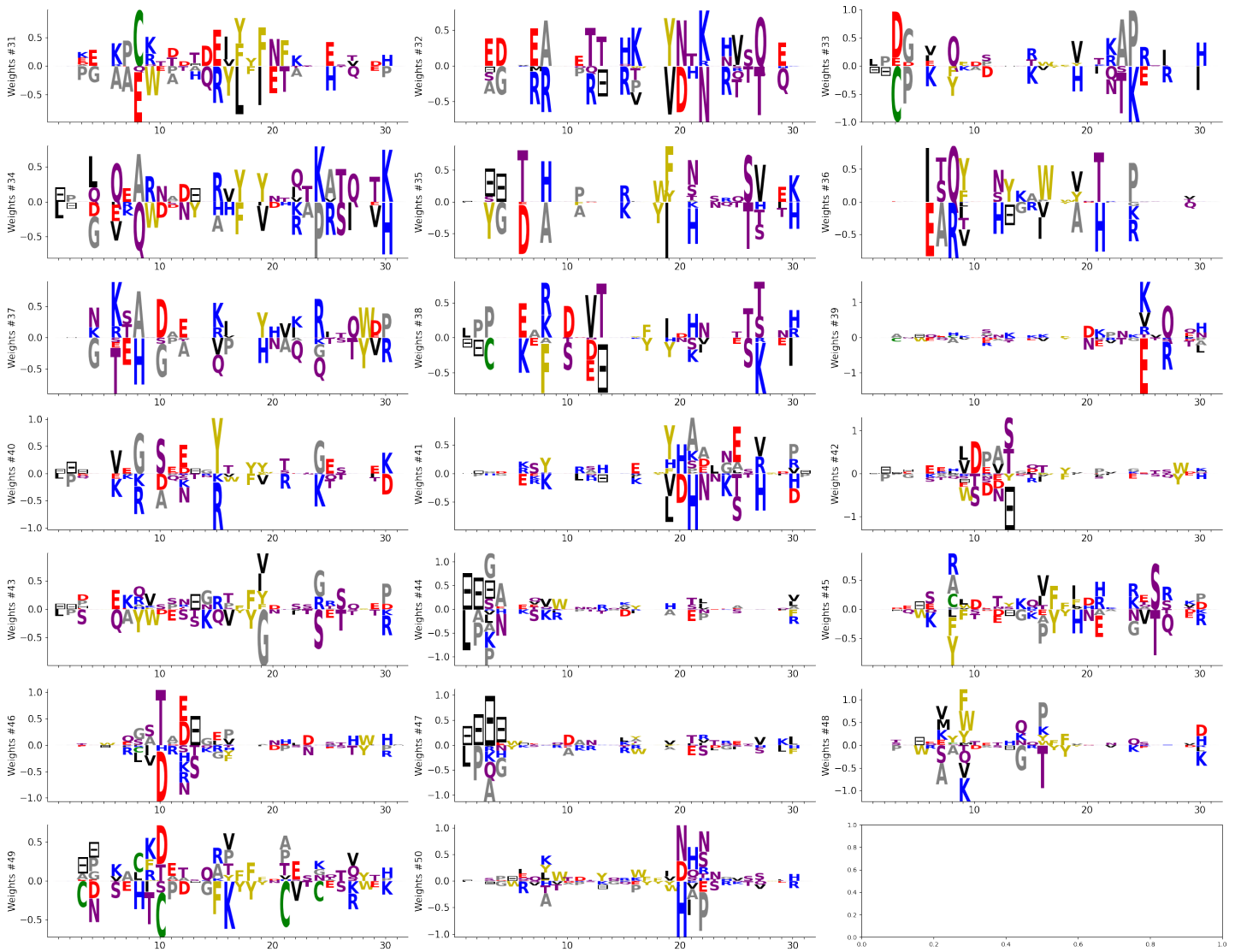


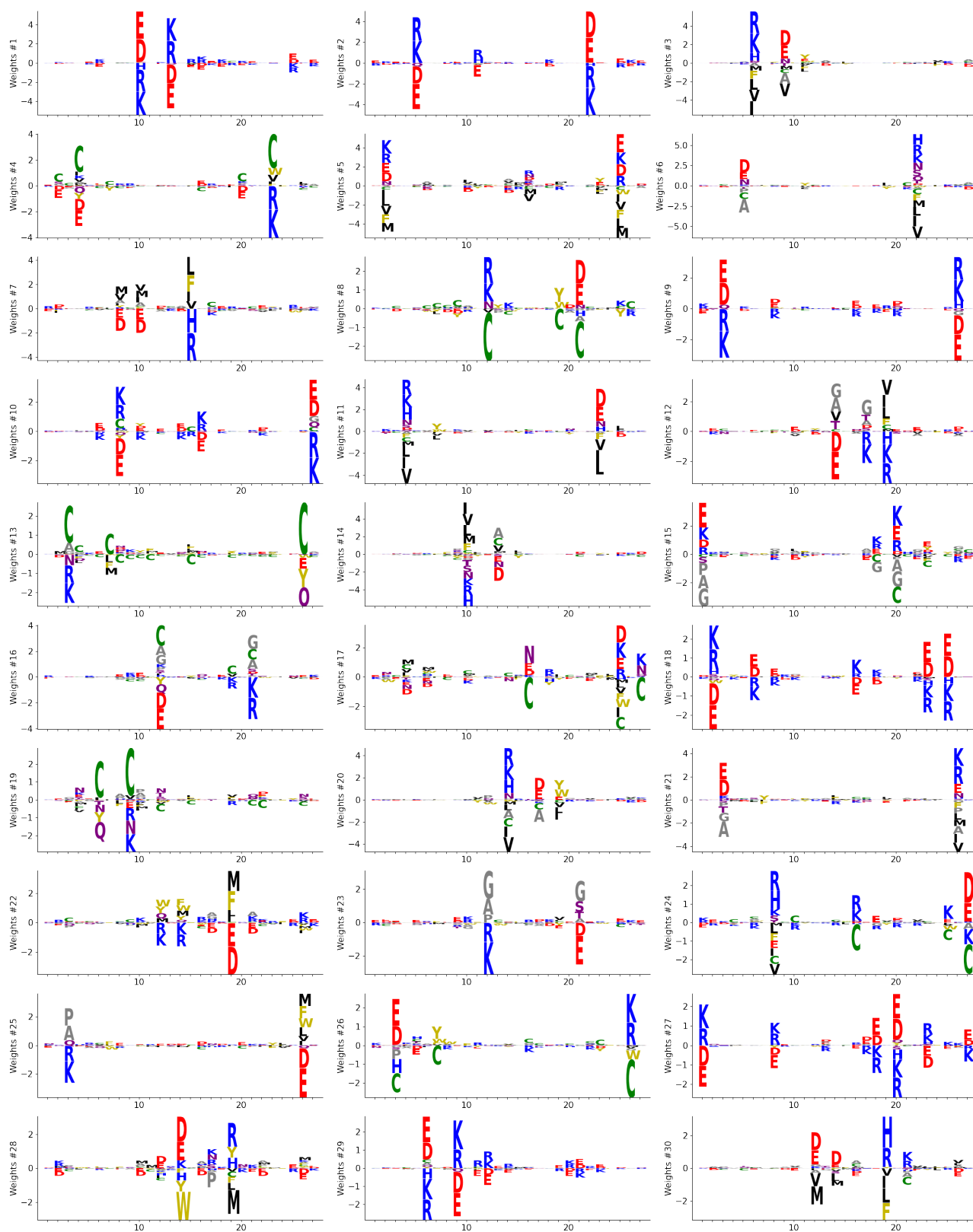
# Appendix A: Weights Logo for the WW domain

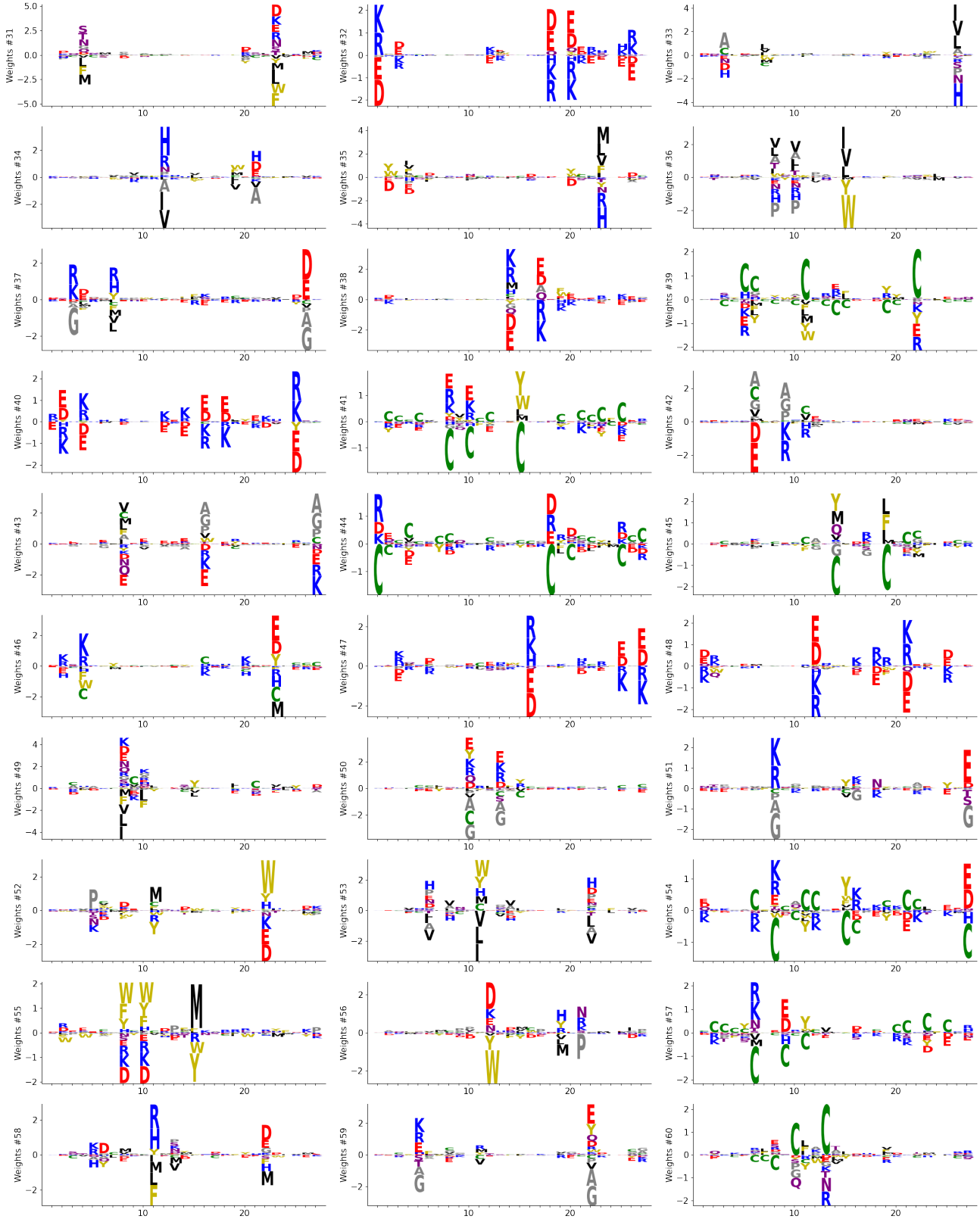


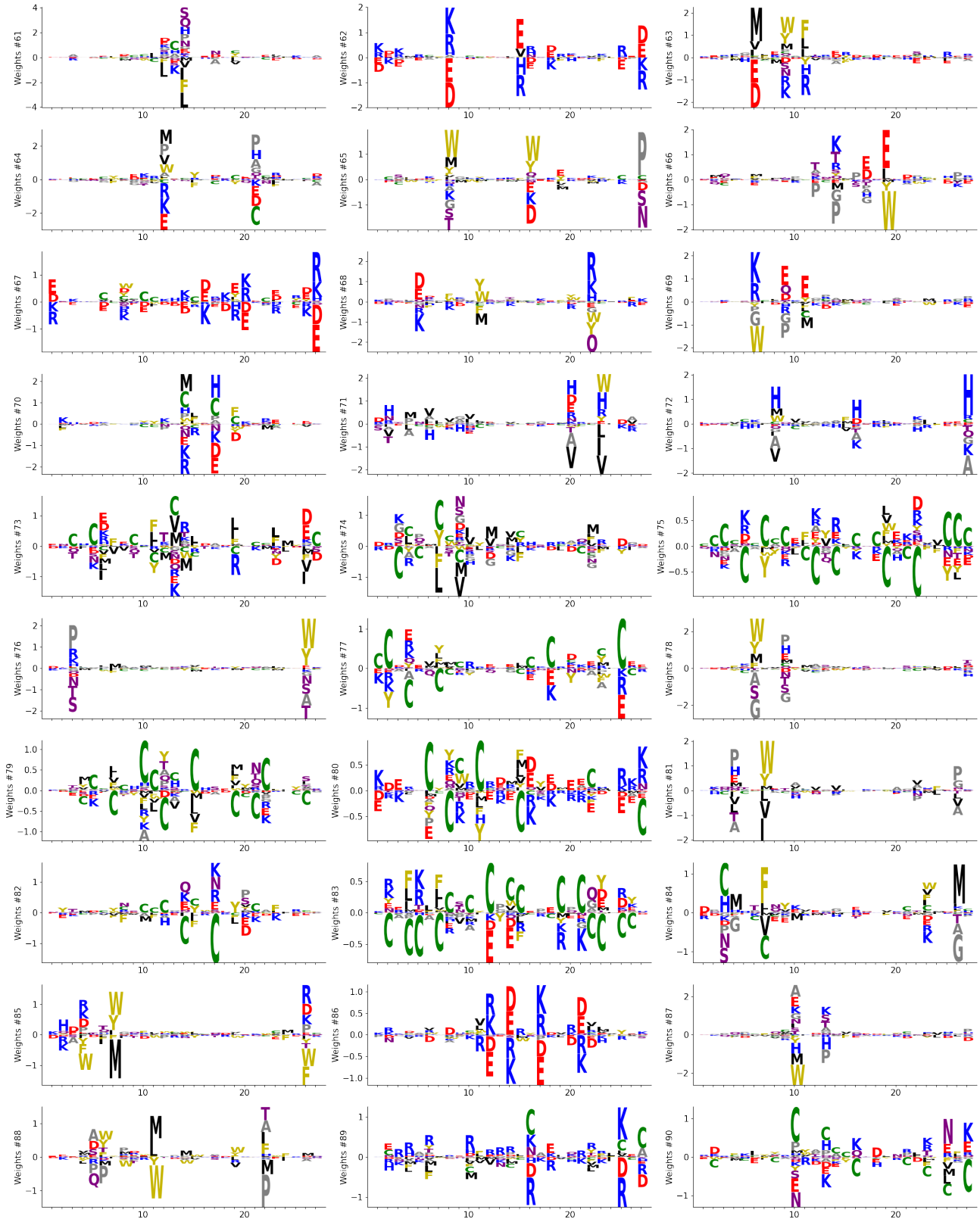
arXiv:2204.10553v2 [q-bio.BM] 24 Oct 2022



## Appendix B: Weights Logo for the Lattice Proteins









# Mutational paths with sequence-based models of proteins: from sampling to mean-field characterisation

Eugenio Mauri, Simona Cocco, Rémi Monasson<sup>1</sup>

<sup>1</sup>Laboratory of Physics of the Ecole Normale Supérieure, CNRS UMR 8023 and PSL Research, Sorbonne Université, 24 rue Lhomond, 75231 Paris cedex 05, France

(Dated: October 25, 2022)

Identifying and characterizing mutational paths is an important issue in evolutionary biology and in bioengineering. We here introduce a generic description of mutational paths in terms of the goodness of sequences and of the mutational dynamics (how sequences change) along the path. We first propose an algorithm to sample mutational paths, which we benchmark on exactly solvable models of proteins in silico, and apply to data-driven models of natural proteins learned from sequence data with Restricted Boltzmann Machines. We then use mean-field theory to characterize the properties of mutational paths for different mutational dynamics of interest, and show how it can be used to extend Kimura’s estimate of evolutionary distances to sequence-based epistatic models of selection.

*Introduction.* Designing proteins with controlled properties, such as stability, binding affinity and specificity is a central goal in bioengineering. Directed evolution setups result in the discovery of new proteins with enhanced activities or affinities to a specific substrate [1]. Over the past years, much progress was made using data-driven models, intended to capture the relation between protein sequences and functionalities. In particular, unsupervised machine-learning approaches such as Boltzmann Machines (BM) or Variational Auto-Encoders trained on homologous sequence data (defining a protein family) were shown to be robust generative models, able to design new proteins with functionalities comparable to natural proteins [2, 3].

By comparison, the (even) harder problem of designing paths of sequences, interpolating between two homologous proteins has received little attention (Fig. 1), see however [4]. Yet solving this problem would be important in bio-engineering, *e.g.* to help design proteins with gradually changing functionalities. In addition, it would shed light on the navigability of the sequence landscape [5], and on how specificity emerged from ancestral, promiscuous proteins [6]. Informally speaking, a path is a succession of mutants interpolating between two fixed sequences at the edges, such that intermediate proteins maintain good functionality and contiguous sequences along the path differ by few mutations. The latter constraint depends on the objective, *e.g.* producing mutational paths plausible from an evolutionary point of view, or optimized for experimental validations. In particular, due to the huge number of possible paths mutagenesis experiments generally restrict to direct paths going through the  $2^D$  mutants containing the amino acids appearing in the two edge sequences (differing on  $D$  sites), see Fig. 1 [7]. However, constraining paths to be direct may preclude the discovery of better global paths, involving mutations and their reversions and reaching more favorable regions in the sequence space [8] (Fig. 1).

While various methods exist for building transition paths between the minima of a multi-dimensional continuous landscape [9, 10] dealing with discrete configurations requires the development of specific procedures [11]. We hereafter propose a Monte Carlo algorithm

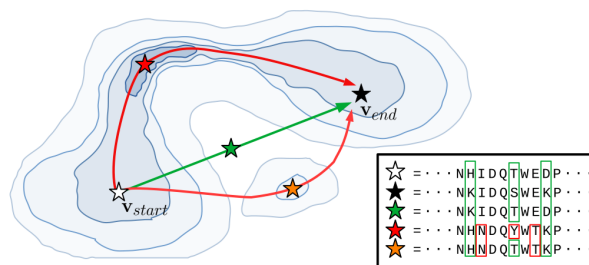


FIG. 1. **Mutational paths between two sequences in the landscape associated to a protein family.** Darker blue levels correspond to increasing values of the protein fitness. Paths joining the start and end sequences are either direct (green: each site carries the amino acid present at the same position in the initial or in the final sequence) or global (red: no restriction on amino acids), making possible the exploration of high fitness regions.

to sample mutational paths in protein landscapes, *e.g.* obtained by Restricted Boltzmann Machines trained on sequence data. We first benchmark our sampling procedure on an exactly solvable model of lattice proteins [12], and demonstrate its capability to find high-quality paths between two proteins belonging to different subfamilies. We then apply our algorithm to the WW domain, a binding module involved in the regulation of protein complexes [13, 14]. The functionality of the sequences along the paths is validated with structure (ligand+protein)-informed software [15]. Last of all we derive a mean-field characterization of paths, tailored to the mutational dynamics of interest. This mean-field theory allows us to efficiently estimate evolutionary distances in the presence of strong epistasis in the selection process, which is not possible with profile models at the basis of most phylogenetic studies [16].

*Definition and sampling of mutational paths.* We assume the sequence landscape is modeled through a probability distribution  $P_{model}(\mathbf{v})$  over amino-acid sequences  $\mathbf{v}$  of length  $N$ . Informally speaking,  $P_{model}$  quantifies the probability that  $\mathbf{v}$  is a member of the protein family of interest, *i.e.* share its common structural and functional properties, and can be learned from homologous

sequence data [17, 18]. For natural protein families, exact expressions for  $P_{model}$  are not available, but approximate distributions can be inferred from multi-sequence alignments (MSA) using unsupervised learning techniques.

Hereafter, we use Restricted Boltzmann Machines (RBM) [19], a class of generative models based on two-layer graphs [20]. RBM define a joint probability distribution of the protein sequence  $\mathbf{v}$  (carried by the visible layer) and of its  $M$ -dimensional latent representation  $\mathbf{h}$  (present on the hidden layer) as

$$P_{RBM} \propto \exp \left( \sum_i g_i(v_i) + \sum_{\mu} h_{\mu} I_{\mu}(\mathbf{v}) - \sum_{\mu} \mathcal{U}_{\mu}(h_{\mu}) \right), \quad (1)$$

where  $I_{\mu}(\mathbf{v}) = \sum_i w_{i,\mu}(v_i)$  is the input to hidden unit  $\mu$ . The  $g_i$ 's and  $\mathcal{U}_{\mu}$ 's are local potentials acting on, respectively, visible and hidden units, and the  $w_{i\mu}$ 's are the interactions between the two layers. They are learned by maximizing the marginal probabilities  $P_{model}(\mathbf{v}) = \int d\mathbf{h} P_{RBM}(\mathbf{v}, \mathbf{h})$  over the sequences  $\mathbf{v}$  in a multi-sequence alignment of the family. While other unsupervised procedures providing approximate  $P_{model}$  can be used, such as Direct Coupling Analysis [17, 18], RBM offer a convenient way to interpret and to visualize the changes in sequences along mutational paths, as we will see below.

We define the probability of a mutational path of  $T$  steps,  $\mathcal{V} = \{\mathbf{v}_1, \mathbf{v}_2, \dots, \mathbf{v}_{T-1}\}$  through

$$\begin{aligned} \mathcal{P}[\mathcal{V} | \mathbf{v}_{start}, \mathbf{v}_{end}] &\propto \prod_{t=1}^{T-1} P_{model}(\mathbf{v}_t) \times \\ &\pi(\mathbf{v}_{start}, \mathbf{v}_1) \times \prod_{t=1}^{T-2} \pi(\mathbf{v}_t, \mathbf{v}_{t+1}) \times \pi(\mathbf{v}_{T-1}, \mathbf{v}_{end}) \quad (2) \end{aligned}$$

where the 'transition' factor  $\pi(\mathbf{v}, \mathbf{v}')$  increases with the similarity between the sequences  $\mathbf{v}, \mathbf{v}'$ . As an illustration we may choose  $\pi = 1$  if the two sequences are identical,  $e^{-\Lambda}$  if they differ by one mutation (with  $\Lambda > 0$ ), and 0 if they are two or more mutations apart. This choice generates 'continuous' paths, along which successive sequences differ by one mutation at most. Other choices for  $\pi$ , more plausible from an evolutionary point of view will be introduced below.

The probability  $\mathcal{P}(\mathcal{V})$  can be sampled as follows. Starting from a path  $\mathcal{V}^0$ , we randomly pick up an intermediate sequences  $\mathbf{v}_t$  and attempt at mutating one amino acid, under the constraint that the Hamming distances of the trial sequence  $\mathbf{v}'$  with  $\mathbf{v}_{t-1}$  and  $\mathbf{v}_{t+1}$  be at most 1. The mutation is then rejected or accepted, *i.e.*  $\mathbf{v}_t \leftarrow \mathbf{v}'$  according to detailed balance. Note that for global paths amino acids can take any values. For direct paths each amino acid has to coincide with the one either in  $\mathbf{v}_{start}$  or in  $\mathbf{v}_{end}$  on the same site, and the length  $T$  of the path matches the Hamming distance  $D = N(1 - q(\mathbf{v}_{start}, \mathbf{v}_{end}))$  between the two edge sequences. To improve the quality of the sampled mutational paths we introduce a fictitious inverse temperature  $\beta$  and resort to simulated annealing. We then sample

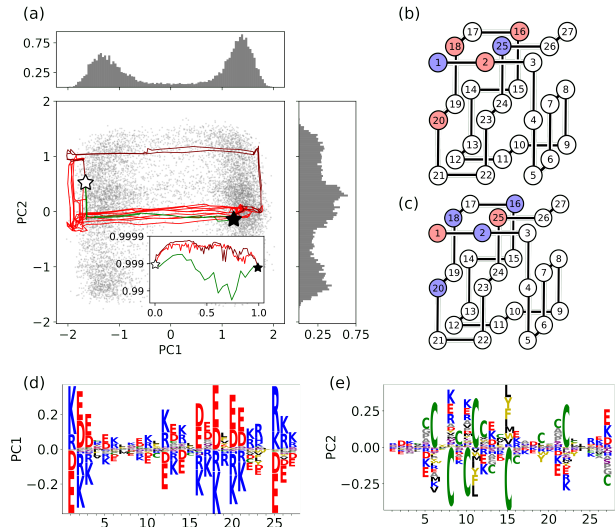


FIG. 2. **Mutational paths for lattice proteins**, joining sequences  $\star = \text{DRGIQCLAQMF EKEMRKKRRCYLECD}$  and  $\blackstar = \text{RECCAVCHQRFKDKIDEDYEDAWLKC N}$  belonging to the family with structure shown in (b) and (c). Red and blue colors respectively correspond to negatively and positively charged amino acids. Cysteine is denoted by a green C. (a) Projections of  $10^4$  LP sequences in the family (grey dots) along the top two PC of their correlation matrix. Green lines represent direct paths, while red and maroon lines show some global paths sampled from Eq. (2); here, we set inverse temperature  $\beta = 3$  and the mutation penalty  $\Lambda = 2$ , while the length of the direct and global paths are respectively  $T_{direct} = 24$ ,  $T_{global} = 82$ . The relative numbers of maroon (2) and red (10) paths respect the statistics over all sampled paths. Sides: histograms of projections along PC1 (top) and PC2 (right). Inset: folding probability  $p_{nat}$  along each path vs. number of mutations/ $T$ . (b,c) Structure of the family. Sequences having opposite alternating configurations of charges along PC1 fold equally well. (d,e) Sequence logos of the top two PCs.

paths from  $\mathcal{P}[\mathcal{V}]^\beta$ , where the value of  $\beta$  is initially very small and progressively ramped up to some target value. The complete procedure and the proof of detailed balance are given in Supplemental Material, Sec. ??.

*Benchmarking mutational path sampling on in silico proteins.* We benchmark the performances of our MC procedure on a model of Lattice Proteins (LP) [12, 21]. In LP, sequences of 27 amino acids may fold into  $\simeq 10^5$  different self-avoiding conformations going through the nodes of a  $3 \times 3 \times 3$  cubic lattice. The sequence landscape associated to a structure  $\mathbf{S}$  (Fig. 2(a)) is defined by the probability  $p_{nat}(\mathbf{v} | \mathbf{S})$  that a sequence  $\mathbf{v}$  has  $\mathbf{S}$  as its native fold;  $p_{nat}$  can be exactly computed from the energies of interactions between adjacent amino acids, see Supplemental Material, Sec. ?? for details.

We first generate many sequences  $\mathbf{v}$  with high  $p_{nat}$  values for the fold  $\mathbf{S}$  of Figs. 2(b,c) following the procedure of [22]. We next compute the top two Principal Components (PC) of these sequence data using one-hot encoding (Figs. 2(d,e)): PC1 corresponds to an extended electrostatic mode, and PC2 identifies possible Cys-Cys bridges. Projecting the sequences onto these two PCs re-

veals two sub-families separated along PC1 (Fig. 2(a)), associated to opposite chains of alternating charges along the electrostatic mode (Figs. 2(b,c)). We will use our path sampling procedure to interpolate between the two sub-families, see start (white star) and end (black star) sequences in Fig. 2(a).

To mimick the approach followed for natural proteins we train a RBM on the LP sequence data generated above, to infer an approximate expression for  $p_{nat}$  from the data; see Supplemental Material, Sec. ?? for details about the inference of the RBM model. We then use our sampling algorithm to produce global mutational paths, see Fig. 2(a). The algorithm is able to find excellent global mutational paths in terms of the ground truth folding probability  $p_{nat}$  (insert Fig. 2(a)). By fixing the target inverse temperature  $\beta$  to a value larger than one, we are able to obtain  $p_{nat}$  values along the path higher than those of the sequences at the extremities. Repeated runs of the sampling procedure give different paths that cluster into two classes, shown in red and maroon in Fig. 2(a). While few global paths exploit a transient introduction of Cys-Cys interaction to stabilize the structure while flipping the electrostatic residues (marron cluster); most (red cluster) introduce additional stabilizing electrostatic contacts along the path (red cluster). See Supplemental Material, Sec ?? for details.

*Mutational path sampling from data-driven models of natural proteins.* We next show that our path sampling procedure can be applied to natural proteins. To do so we train a RBM from MSA data of the WW family, a protein domain binding specifically proline-rich peptides [13, 23] and sample mutational paths, either global or direct, between the Human YAP1 domain and three natural sequences known to have different binding specificities [26]. Figure 3(a) shows some sampled paths in the 2-dimensional space spanned by the inputs  $I(\mathbf{v})$  (see Eq. 1) to two RBM hidden units chosen to cluster natural WW sequences depending on their binding specificities [20]. Figures 3(b,c) show the probabilities of sequences along global and direct paths are comparable to the ones of natural proteins, with significantly higher values for global paths. We then use AlphaFold [27] to assess the quality of the intermediates sequences; AlphaFold is able to predict the phenotypic effects of mutations [28], and to compare the resulting structures to natural folds through Template Modelling scores (TM-score) [29], ranging from 0 -unrelated proteins- up to 1 -perfect match. We obtain TM-score  $> 0.5$ , indicating a high similarity between the folds of sequences sampled along the path and of natural WW, see Supplemental Material, Sec. ?? for details.

We next estimate binding affinity for each class using ProteinMPNN [15], an autoregressive structural-based probabilistic model that takes as input a backbone structure of a protein-ligand complex and predicts the affinity score of a putative protein sequence. Here, we use complexes of known natural WW domains of classes I, II/III, IV with their cognate peptides, see Fig. 3(h) and Supplemental Material, Sec. ?? for details. As expected, along the I  $\rightarrow$  II/III path the affinities of sequences to

class I (II/III) -cognate peptides decrease (increase), see Fig. 3(d). Interestingly, Fig. 3(e) shows the existence of a region on the I  $\rightarrow$  IV path in which the predicted

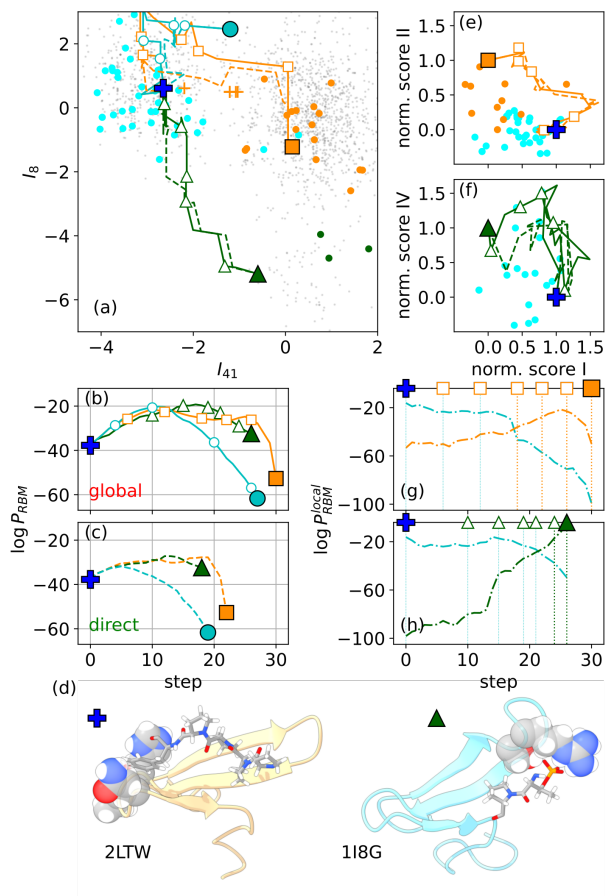


FIG. 3. **Mutational paths of the WW domain** using RBM trained on the PFAM PF00397 family, see Supplemental Material, Sec. ?? for details about implementation. (a) Natural sequences  $\mathbf{v}$  (grey dots) projected in the plane of inputs  $I$  of two hidden units selected to cluster sequences according to the types of ligands they bind: I (cyan), II/III (orange), IV (green), see classification in [23]. Blue cross represents the YAP1 domain. Lines shows the projection of six representative paths (dashed: direct, solid: global) connecting YAP1 to sequences in classes I (circle), II/III (square; note the vicinity of the direct path with variants of YAP1 -orange crosses- tested in [24]) and IV (triangle). Empty symbols show intermediate sequences tested also with AlphaFold. All the sequences standing for these symbols are shown in Supplemental Material, Sec. ?? . Parameters:  $\beta = 3$ ,  $\Lambda = 0.1$ . (b)-(c) Log  $P_{RBM}$  for sequences along global and direct paths. (d) Complexes (WW domain and cognate peptides) for classes I (blue cross) and IV (green triangle) [25]. The atoms corresponding to the two binding pockets are highlighted in the structures. (e)-(f) Normalized ProteinMPNN scores for binding affinity, see Supplemental Material, Sec. ?? .  $x$ -axis measures the affinity to class I reference structure while  $y$ -axes show affinity to classes II/III (e) and IV (f) reference structure respectively. (g)-(h) Log-likelihood along the global paths from I to II (g) and from I to IV (h) according to RBM trained on class-specific sequence data (Cyan: I, Orange: II/III, Green: IV).

affinities with respect to both complexes are high. This promiscuity may be favored by the fact that class I and IV cognate peptides bind two distinct loops of the WW domain (Fig. 3(h)). To further assess the specificity of sequences on the sampled path, we train class-specific RBM models from sequences in the associated quadrants in Fig. 3(a). The cross-overs between the log-likelihoods of the class-specific RBMs in Fig. 3(g,h) locate the specificity switches along the  $I \rightarrow \text{II/III}$  and  $I \rightarrow \text{IV}$  paths.

*Mean-field theory of mutational paths.* To better characterize the typical properties of mutational paths we resort to mean-field theory, by formally sending  $N \rightarrow \infty$ , while keeping the number  $T$  of steps finite. To allow for  $\mathcal{O}(N)$  mutations between contiguous sequences we write the transition factor in Eq. 2 as  $\pi(\mathbf{v}, \mathbf{v}') = e^{-N\Phi(q)}$ , where the potential  $\Phi$  is a decreasing function of the overlap  $q = \frac{1}{N} \sum_i \delta_{v_i, v'_i}$ .  $\Phi$  controls the elastic properties of the path, and will be made precise below.

Mean-field theory exploits the bipartite nature of the RBM architecture and allows us to monitor two sets of order parameters characterizing the paths  $\mathcal{V}$ : the mean values of the hidden-unit inputs,  $m_t^\mu = \frac{1}{N} \langle I_\mu(\mathbf{v}_t) \rangle$ , and of the overlaps (fraction of conserved amino acids between successive sequences),  $q_t = \frac{1}{N} \sum_i \langle \delta_{v_{i,t}, v_{i,t+1}} \rangle$ ; here,  $\langle \cdot \rangle$  denotes the average over  $\mathcal{P}(\mathcal{V})^\beta$ .

The  $T \times (M + 1)$  order parameters  $m_t^\mu$  and  $q_t$  are determined through minimization of the path free-energy density  $f_{\text{path}}$ , see Supplemental Material, Sec. ??, with

$$f_{\text{path}}(\{m_t^\mu\}, \{q_t\}) = - \sum_{t,\mu} (\Gamma_\mu(m_t^\mu) - m_t^\mu \Gamma'_\mu(m_t^\mu)) \quad (3)$$

$$+ \sum_t (\Phi(q_t) - q_t \Phi'(q_t)) - \frac{1}{\beta N} \sum_i \ln Z_i(\{m_t^\mu\}, \{q_t\}).$$

Here,  $\Gamma_\mu(m) = \frac{1}{N} \ln \int dh e^{N m h - \mathcal{U}_\mu(h)}$  and  $Z_i$  is the following site-dependent partition function,

$$Z_i(\{m_t^\mu\}, \{q_t\}) = \sum_{\{v_t\}} \exp \left( \beta \sum_t g_i(v_t) + \right.$$

$$\left. + \beta \sum_{t,\mu} \Gamma'_\mu(m_t^\mu) w_{i\mu}(v_t) - \beta \sum_t \Phi'(q_t) \delta_{v_t, v_{t+1}} \right). \quad (4)$$

$Z_i$  can be efficiently estimated through products of transfer matrices, of sizes  $21 \times 21$  for global paths, and  $2 \times 2$  for direct paths. The expression of  $f_{\text{path}}$  is exact for sequence length  $N \rightarrow \infty$  and the numbers of hidden units,  $M$ , and of steps,  $T$  remain finite, and is an accurate approximation even in the cases of LP ( $N = 27$ ) and WW ( $N = 31$ ).

*Choice of the elastic potential.* The potential  $\Phi$  can enforce continuity (Cont) requirements, e.g. successive sequences along the path differ by, say,  $K$  mutations at most, or mimic the evolutionary (Evo) dynamics of natural sequences through stochastic mutations.

In the Cont scenario the potential  $\Phi$  should forbid large jumps along the paths. We thus consider a hard-wall

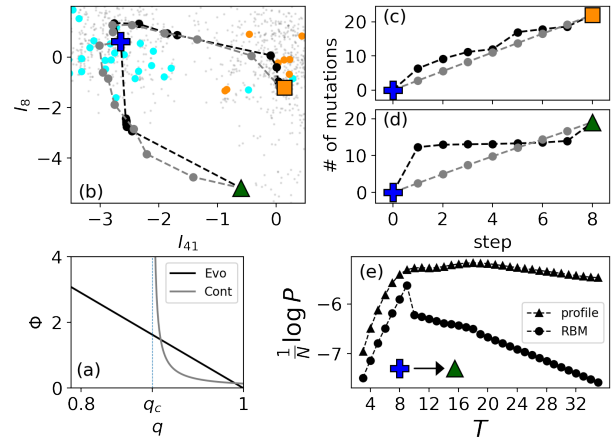


FIG. 4. **Mean-field theory of mutational paths** for the RBM model trained on WW domain. (a) Sketches of the potentials  $\Phi_{\text{Evo}}$  (black) and  $\Phi_{\text{Cont}}$  (gray) vs.  $q$ . (b) Same two-dimensional representation as in Fig. 3(a) for the mean-field paths with Evo (black lines) and Cont (gray lines) potentials. (c)-(d) Cumulative numbers of mutations vs.  $t$ . Here,  $\mu = 10^{-5}$  and  $\gamma = 0.9$ , so that the cumulative numbers match for  $t = T$ . (e) Log-probability of joining class I and class IV natural WW domains in  $T$  steps with the profile (triangles) and RBM (circles) models. Jumps signal the onset of several new mutations, e.g. 4 in the mean-field free path at  $T = 10$ .

repulsive potential (Fig. 4(a)),

$$\Phi_{\text{Cont}}(q) = \frac{\phi(T)}{q - q_c(T)} \text{ if } q_c(T) < q \leq 1, +\infty \text{ otherwise.} \quad (5)$$

The location of the hard wall,  $q_c(T) = 1 - \gamma/T$ , allows the path to explore at most  $K \equiv T \times N(1 - q_c) = \gamma N$  mutations in  $T$  steps. Choosing  $\gamma \geq D/N$  ( $D$  being the Hamming distance between  $\mathbf{v}_{\text{start}}$  and  $\mathbf{v}_{\text{end}}$ ), is therefore sufficient to interpolate between the two edge sequences, with larger values of  $\gamma$  authorizing more flexible paths. The proportionality constant  $\phi(T) = 1/T^2$  is set to guarantee the existence of a well defined limit for large  $T$ .

In the Evo scenario, the potential should emulate Kimura's model of neutral evolution [30], while the  $P_{\text{model}}$  factors in Eq. 2 correspond to selection. Denoting the mutation rate (over a time interval corresponding to one step of the path) by  $\mu$  we show in Supplemental Material, Sec. ??, that the potential is given by [31]

$$\Phi_{\text{Evo}}(q) = (1 - q) \ln \left( 1 + \frac{A}{e^{\mu A/(A-1)} - 1} \right), \quad (6)$$

where  $A = 21$  is the number of amino acids plus the gap state. It is linearly decreasing with  $q$ , see Fig. 4(a).

Cont and Evo mean-field paths between class-specific WW domains are shown in Fig. 4(b); both follow similar traces in the specificity plane, in agreement with the sampled paths in Fig. 3(a). However, the distribution of mutations along the paths largely differ between the two scenarios, compare Fig. 4(c-d). Mutations are homogeneously spread along the Cont path, with  $\simeq N\gamma/T$  mutations at each step. Conversely, the Evo path is highly

heterogeneous, with some steps accumulating many mutations and others barely any, see Supplemental Material, Sec. ?? for the list of consensus sequences computed with the mean-field theory. Interestingly, most steps along the Evo path I→IV are concentrated in the region characterized by promiscuous sequences binding both ligand classes as mentioned above, which could then correspond to ancestral, not yet specialized sequences [6].

*Mean-field based estimation of evolutionary distance.* As an application of our mean-field approach we show how it can be used to estimate evolutionary distances between sequences with complex data-driven models, including epistatic interactions between residues. The probability that sequence  $\mathbf{v}_{end}$  be reached after  $T$  steps of stochastic mutations with rate  $\mu$  starting from  $\mathbf{v}_{start}$  is given by

$$P(\mathbf{v}_{start} \rightarrow \mathbf{v}_{end}|T) \sim \exp \left[ -N(f_{path}^{constrained} - f_{path}^{free}) \right], \quad (7)$$

where  $f_{path}^{constrained}$  is the free energy in Eq. 4 (with potential  $\Phi_{Evo}$ ) minimized under boundary conditions matching both  $\mathbf{v}_{start}$  and  $\mathbf{v}_{end}$ , while  $f_{path}^{free}$  is obtained by releasing the boundary condition at the end extremity of the path. Details on the numerical optimization are given in Supplementary Material, Sec. ??.

This probability can be computed as a function of  $T$  to determine the optimal time (evolutionary distance)  $T^*$  at which it is maximal. For purely neural evolution,  $f_{path}^{free} = 0$  and the probability  $P(\mathbf{v}_{start} \rightarrow \mathbf{v}_{end}|T)$  can be exactly computed;  $T^*$  then coincides with the predictions of Kimura’s theory of neutral evolution [30], see Supplemental Material, Sec. ?. Kimura’s result can be easily extended to the case of profile models [16], where selection acts independently from site to site, see Fig. 4(e) for an illustration of WW. Our mean-field theory theory allows us to go well beyond profile models, and to compute the probability  $P$  in the presence of epistatic effects in the RBM model inferred from WW sequence data. Figure 4(e) shows that the evolutionary distance  $T^*$  may then substantially differ from its profile counterpart, showing the effectiveness of our mean-field approach to deal with complex sequence models.

*Conclusion.* In this work we have introduced numerical and analytical tools to sample and characterize mutational paths in data-driven models (RBM) of protein sequences. Our sampling algorithm was illustrated on the WW domain, but can be applied to longer enzymes, with  $> 100$  amino acids. We have validated the structural and functional properties of intermediate sequences along the paths with AlphaFold and ProteinMPNN, two deep-learning-based computational methods. A potentially interesting biological finding is that the path interpolating between specificity classes I and IV go through a region apparently deprived of natural sequences, albeit corresponding to high RBM likelihood[32] and high ProteinMPNN scores for both ligands (Fig. 3). These intermediate sequences are putatively unspecialized, and possibly similar to ancestral proteins. Investigating experimentally their properties would be very interesting.

In addition, we have shown how RBM models are amenable to mean-field analysis, through the determination of the time-trajectory of the mean inputs to the hidden units and of the overlaps between successive sequences along the path. Mean field is a powerful computational scheme in the presence of strong interactions between residues, *e.g.* to estimate evolutionary distances. This result opens the way to ancestral reconstruction and to the prediction of phylogenetic trees [16] with data-driven, epistatic models.

*Acknowledgements.* We are particularly grateful to J. Tubiana for his help on the use of ProteinMPNN. We also thank M. Bisardi, A. Di Gioacchino, A. Murugan, and F. Zamponi for discussions. This work was supported by the ANR-17 RBMPro and ANR-19 Decrypted CE30-0021-01 projects. E.M. is funded by a ICFP Labex fellowship of the Physics Department at ENS.

- 
- [1] O. Kuchner and F. H. Arnold, Trends in Biotechnology **15**, 523 (1997).
  - [2] W. P. Russ, M. Figliuzzi, C. Stocker, P. Barrat-Charlaix, M. Socolich, P. Kast, D. Hilvert, R. Monasson, S. Cocco, M. Weigt, and R. Ranganathan, Science **369**, 440 (2020).
  - [3] A. Hawkins-Hooker, F. Depardieu, S. Baur, G. Couairon, A. Chen, and D. Bikard, PLOS Computational Biology **17**, 1 (2021).
  - [4] P. Tian and R. B. Best, PLOS Computational Biology **16**, 1 (2020).
  - [5] S. F. Greenbury, A. A. Louis, and S. E. Ahnert, bioRxiv (2021), 10.1101/2021.10.11.463990.
  - [6] O. Khersonsky and D. S. Tawfik, Annual Review of Biochemistry **79**, 471 (2010).
  - [7] F. J. Poelwijk, M. Socolich, and R. Ranganathan, Nat. Commun. **10**, 1 (2019).
  - [8] N. C. Wu, L. Dai, C. A. Olson, J. O. Lloyd-Smith, and R. Sun, eLife **5**, e16965 (2016).
  - [9] E. Vanden-Eijnden *et al.*, Annual review of physical chemistry **61**, 391 (2010).
  - [10] P. G. Bolhuis, D. Chandler, C. Dellago, and P. L. Geissler, Annual review of physical chemistry **53**, 291 (2002).
  - [11] T. Mora, A. M. Walczak, and F. Zamponi, Physical Review E **85**, 036710 (2012).
  - [12] K. F. Lau and K. A. Dill, Macromolecules **22**, 3986 (1989).
  - [13] M. Sudol, Progress in biophysics and molecular biology **65**, 113 (1996).
  - [14] M. Socolich, S. Lockless, W. Russ, H. Lee, K. Gardner, and R. Ranganathan, Nature **437**, 512 (2005).
  - [15] J. Dauparas, I. Anishchenko, N. Bennett, H. Bai, R. J. Ragotte, L. F. Milles, B. I. Wicky, A. Courbet, R. J. de Haas, N. Bethel, *et al.*, Science, eadd2187 (2022).
  - [16] J. Felsenstein and J. Felsenstein, *Inferring phylogenies*, Vol. 2 (Sinauer associates Sunderland, MA, 2004).
  - [17] F. Morcos, A. Pagnani, B. Lunt, A. Bertolino, D. S. Marks, C. Sander, R. Zecchina, J. N. Onuchic, T. Hwa, and M. Weigt, Proceedings of the National Academy of Sciences **108**, E1293 (2011).
  - [18] S. Cocco, C. Feinauer, M. Figliuzzi, R. Monasson, and M. Weigt, Reports on Progress in Physics **81**, 032601 (2018).

- [19] A. Fischer and C. Igel, in *Iberoamerican congress on pattern recognition* (Springer, 2012) pp. 14–36.
- [20] J. Tubiana, S. Cocco, and R. Monasson, *eLife* **8**, e39397 (2019).
- [21] E. I. Shakhnovich and A. M. Gutin, *Proceedings of the National Academy of Sciences* **90**, 7195 (1993), <https://www.pnas.org/doi/pdf/10.1073/pnas.90.15.7195>.
- [22] H. Jacquin, A. Gilson, E. Shakhnovich, S. Cocco, and R. Monasson, *PLOS Computational Biology* **12**, 1 (2016).
- [23] A. Zarrinpar and W. A. Lim, *Nature structural biology* **7**, 611 (2000).
- [24] X. Espanel and M. Sudol, *Journal of Biological Chemistry* **274**, 17284 (1999).
- [25] E. F. Pettersen, T. D. Goddard, C. C. Huang, E. C. Meng, G. S. Couch, T. I. Croll, J. H. Morris, and T. E. Ferrin, *Protein Science* **30**, 70 (2021).
- [26] M. Sudol and T. Hunter, *Cell* **103**, 1001 (2000).
- [27] J. Jumper, R. Evans, A. Pritzel, T. Green, M. Figurnov, O. Ronneberger, K. Tunyasuvunakool, R. Bates, A. Žídek, A. Potapenko, *et al.*, *Nature* **596**, 583 (2021).
- [28] J. M. McBride, K. Polev, V. Reinharz, B. A. Grzybowski, and T. Tlusty, arXiv preprint arXiv:2204.06860 (2022).
- [29] Y. Zhang and J. Skolnick, *Proteins: Structure, Function, and Bioinformatics* **57**, 702 (2004).
- [30] M. Kimura, *The neutral theory of molecular evolution* (Cambridge University Press, 1983).
- [31] I. Leuthäusser, *Journal of statistical physics* **48**, 343 (1987).
- [32] We stress that RBM trained on all sequence data, mixing several classes, cannot detect a change of specificity, contrary to RBM models restricted to each class (Fig. 3(g,h)).

# Supplemental Material

## Mutational paths with sequence-based models of proteins: from sampling to mean-field characterisation

Eugenio Mauri, Simona Cocco, Remi Monasson

October 25, 2022

### 1 Path sampling algorithm

#### 1.1 Detailed description

We introduce below the details of the sampling procedure we use to obtain paths connecting two fixed sequences in a landscape described by the probability distribution  $P_{model}$ . Starting from a path  $\{\mathbf{v}_t\}$ , we look at intermediate sequences (starting from  $t = 1$ ) and propose a mutation with the constraint that the Hamming distance between  $\mathbf{v}_{t-1}$  and  $\mathbf{v}_{t+1}$  is not greater than 1. We accept this move with a probability fixed to ensure detail balance. Different cases have to be considered, depending on the Hamming distance  $D_H$  between the new attempted sequence and existing ones (note that hereafter we define  $\pi(\mathbf{v}, \mathbf{v}') = \exp[-N\Phi(\frac{1}{N} \sum_i \delta_{v_i, v'_i})]$ ):

- $D_H(\mathbf{v}_{t-1}, \mathbf{v}_{t+1}) = 0$ . In this case the new sequence  $\mathbf{v}'_t$  can have a single mutation at any site, compared with the two adjacent sequences along the path. Hence, we first draw a random site  $i$ , then we propose a new sequence  $\hat{\mathbf{v}}_{t-1}$  amino-acids for that site  $\hat{v}_t^i$  drawn from the distribution  $\propto P_{model}^\beta(\cdot | \mathbf{v}_{t-1}^{\setminus i})$ , where the amino acids are fixed on all the sites different from  $i$ . Then if the old sequence  $\mathbf{v}_t$  already had a mutation with respect to  $\mathbf{v}_{t-1}$  at given site  $j$ , we accept the new mutated sequence  $\hat{\mathbf{v}}_t$  (which is equal to  $\mathbf{v}_{t-1}$  apart from the amino acid at site  $i$ ) with a probability

$$p_{acc}(\mathbf{v}_t \rightarrow \hat{\mathbf{v}}_t) = \min \left( 1, \frac{\pi(\mathbf{v}_{t-1}, \hat{\mathbf{v}}_t)^{2\beta} \sum_z P_{model}^\beta(M_i^z \mathbf{v}_{t-1})}{\pi(\mathbf{v}_{t-1}, \mathbf{v}_t)^{2\beta} \sum_z P_{model}^\beta(M_j^z \mathbf{v}_{t-1})} \right), \quad (1)$$

where  $M_i^z$  indicates the mutation  $z$  at site  $i$ . If  $\mathbf{v}_t$  or  $\hat{\mathbf{v}}_t$  are equal to  $\mathbf{v}_{t-1}$ , then the acceptance probability is  $p_{acc}(\mathbf{v}_t \rightarrow \hat{\mathbf{v}}_t) = \min(1, \pi(\mathbf{v}_{t-1}, \hat{\mathbf{v}}_t)^{2\beta} / \pi(\mathbf{v}_{t-1}, \mathbf{v}_t)^{2\beta})$ .

- $D_H(\mathbf{v}_{t-1}, \mathbf{v}_{t+1}) = 1$ . In this case the new sequence  $\hat{\mathbf{v}}_t$  can have a single mutation only at the site  $i$  where  $\mathbf{v}_{t-1}$  and  $\mathbf{v}_{t+1}$  are different. At that site, we propose a new mutation from the distribution  $\propto P_{model}^\beta(\cdot | \mathbf{v}_{t-1}^{\setminus i})$  and accept it with probability  $p_{acc} = \exp[-\Lambda\beta(D_H(\hat{\mathbf{v}}_t, \mathbf{v}_{t-1}) + D_H(\hat{\mathbf{v}}_t, \mathbf{v}_{t+1}) - D_H(\mathbf{v}_t, \mathbf{v}_{t-1}) - D_H(\mathbf{v}_t, \mathbf{v}_{t+1}))]$ .
- $D_H(\mathbf{v}_{t-1}, \mathbf{v}_{t+1}) = 2$ . In this case the previous and subsequent sequence present two mutations at site  $i$  and  $j$ . The new sequence  $\hat{\mathbf{v}}_t$  can be of two forms: it can have the same mutation of  $\mathbf{v}_{t+1}$  (with respect to  $\mathbf{v}_{t-1}$ ) at site  $i$  or at site  $j$ . Hence, we extract one of the two possibilities with a probability weighted accordingly with  $P_{model}^\beta(\hat{\mathbf{v}}_t)$ .

#### 1.2 Proof of detailed balance

To prove that dynamics given by our algorithm of path sampling converges to the target distribution we have to prove that it respects detailed balance, i.e. the reversibility of each Markov step. We consider the transition from a path  $\{\mathbf{v}_t\}$  to a new path that differ only by one sequence  $\mathbf{v}'_t$  at time  $t$ . we write the detailed balance condition as

$$\begin{aligned} \mathcal{P}_{path}(\{\mathbf{v}_t\})p_{trans}(\mathbf{v}_t \rightarrow \mathbf{v}'_t) &= \mathcal{P}_{path}(\{\mathbf{v}'_t\})p_{trans}(\mathbf{v}'_t \rightarrow \mathbf{v}_t) \\ \pi(\mathbf{v}_{t-1}, \mathbf{v}_t)\pi(\mathbf{v}_t, \mathbf{v}_{t+1})P_{model}(\mathbf{v}_t)p_{trans}(\mathbf{v}_t \rightarrow \mathbf{v}'_t) &= \pi(\mathbf{v}_{t-1}, \mathbf{v}'_t)\pi(\mathbf{v}'_t, \mathbf{v}_{t+1})P_{model}(\mathbf{v}'_t)p_{trans}(\mathbf{v}'_t \rightarrow \mathbf{v}_t) \end{aligned} \quad (2)$$

If  $D_H(\mathbf{v}_{t-1}, \mathbf{v}_{t+1}) = 0$ , the new sequence can have a mutation at any site  $i$  compared to its neighbour  $\mathbf{v}_{t-1}$ , while  $\mathbf{v}_t$  will have the mutation at another site  $j$  (note that  $i$  and  $j$  can be equal. Hence the transition probability in this case will be

$$p_{trans}(\mathbf{v}_t \rightarrow \mathbf{v}'_t) = \frac{1}{N} \frac{P_{model}(\mathbf{v}'_t)}{\sum_{z=1}^Q P_{model}(M_i^z \mathbf{v}_{t-1})} p_{acc}(\mathbf{v}_t \rightarrow \mathbf{v}'_t), \quad p_{trans}(\mathbf{v}'_t \rightarrow \mathbf{v}_t) = \frac{1}{N} \frac{P_{model}(\mathbf{v}_t)}{\sum_{z=1}^Q P_{model}(M_j^z \mathbf{v}_{t-1})} p_{acc}(\mathbf{v}'_t \rightarrow \mathbf{v}_t). \quad (3)$$

By substituting everything in the detailed balance condition we obtain the acceptance probability described in the main paper. This will hold similarly when  $D_H(\mathbf{v}_{t-1}, \mathbf{v}_{t+1}) = 1$  (with  $i = j$ ). For  $D_H(\mathbf{v}_{t-1}, \mathbf{v}_{t+1}) = 2$ , the sequences  $\mathbf{v}_t$  and  $\mathbf{v}'_t$  can either be equal to  $\mathbf{v}_{t+1}$  or  $\mathbf{v}_{t-1}$ , from which the condition presented in the paper descends.

## 2 Lattice Proteins

To benchmark the performances of this MC procedure to find good transition path between two sequences, we test it on Lattice Proteins [LD89], a well known toy-model for protein structure. We consider a protein sequence of 27 amino acids folding into a 3D structure specified as a self-avoiding path over a 3x3x3 lattice where each amino acid occupies one node. The probability of a sequence  $\mathbf{v}$  to fold into a specific structure  $\mathcal{S}$  is given by the interaction energies between amino acids in contact in the structure (i.e. those who occupy neighbouring nodes of the lattice, but are not adjacent in the protein sequence). In particular, the total energy of a sequence with respect to a given structure is given by

$$\mathcal{E}_{LP}(\mathbf{v}|\mathcal{S}) = \sum_{i < j} c_{ij}^{\mathcal{S}} E_{MJ}(v_i, v_j) \quad (4)$$

where  $c^{\mathcal{S}}$  is the contact map ( $c_{ij}^{\mathcal{S}} = 1$  if sites are in contact and 0 otherwise), while the pairwise energy  $E_{MJ}(v_i, v_j)$  represents the amino-acid physico-chemical interactions given by the the Miyazawa-Jernigan knowledge-based potential [MJ96]. The probability to fold into a specific structure is written as

$$p_{nat}(\mathcal{S}|\mathbf{v}) = \frac{e^{-\mathcal{E}_{LP}(\mathbf{v}|\mathcal{S})}}{\sum_{\mathcal{S}'} e^{-\mathcal{E}_{LP}(\mathbf{v}|\mathcal{S}')}}, \quad (5)$$

where the sum is over the entire set of self-avoiding path in the cubic lattice.

The function  $p_{nat}$  represents a suitable landscape that maps each sequence to a score measuring the quality of its folding. To study in more detail this landscape, we will consider an alignment of sequences folding into a specific structure (that we will call  $\mathcal{S}$ ) sampled from a low temperature MC sampling using  $-\beta \log p_{nat}(\cdot|\mathcal{S})$  (with  $\beta = 10^3$ ) as effective energy [JGS<sup>+</sup>16].

## 3 Restricted Boltzmann Machines and training parameter

To study the problem of transition paths we first need a model to infer a landscape from our sequence data set. At this scope, we are going to use Restricted Boltzmann Machines, an unsupervised energy-based model able to learn representations of the data in a two-layer bipartite graph [FI12]. The first "visible" layer represents the protein sequence  $\mathbf{v} = \{v_1, \dots, v_N\}$  where each unit takes one out of 21 possible states (20 amino acids + 1 alignment gap). The second is the "hidden" layer which displays the real-valued representations  $\mathbf{h} = \{h_1, \dots, h_M\}$ . The joint probability distribution for  $\mathbf{v}$  and  $\mathbf{h}$  is

$$P_{RBM}(\mathbf{v}, \mathbf{h}) \propto \exp \left[ \sum_{i=1}^N g_i(v_i) + \sum_{i,\mu} w_{i\mu}(v_i)h_\mu - \sum_{\mu} \mathcal{U}(h_\mu) \right] \quad (6)$$

up to a normalization constant. visible and hidden units are coupled through the matrices  $w_{i\mu}$  and the value of each unit is biased by the local fields  $g_i$  and  $\mathcal{U}_\mu$ . In [TCM19] it has been shown that this model is able to recover statistically relevant

sequence motifs playing crucial roles in the structure and functionality of different protein families. Following their approach, we choose  $\mathcal{U}_\mu$  to be double Rectified Linear Unit (dReLU) potentials of the form

$$\mathcal{U}_\mu(h) = \frac{1}{2}\gamma_{\mu,+}h_+^2 + \frac{1}{2}\gamma_{\mu,-}h_-^2 + \theta_{\mu,+}h_+ + \theta_{\mu,-}h_-, \text{ where } h_+ = \max(h, 0), h_- = \min(h, 0), \quad (7)$$

where we have defined the hyper-parameters  $\gamma_{\mu,\pm}, \theta_{\mu,\pm}$ .

At this point, we need a learning procedure to infer the hyper-parameters that best fit our data. We decided to use a Persistent Contrastive Divergence algorithm [Tie08] which has been shown to be sufficiently good and robust under cautious choice of the regularization hyper-parameters [Tub18a]. The code and the data used to train our RBMs for Lattice Proteins and WW domains can be found in [Tub18b]. The hyper-parameters used for learning are the following:

- For WW ( $N=31$ ):
  - $M = 50$
  - Batch size = 100
  - Number of epochs = 500
  - Learning rate =  $5 \times 10^{-3}$  (which has a decay rate of 0.5 after 50% of iterations)
  - $L_1b$  regularization = 0.25
  - Number of MC step between each update = 10
- For Lattice Protein ( $N=27$ ):
  - $M = 100$
  - Batch size = 100
  - Number of epochs = 100
  - Learning rate =  $5 \times 10^{-3}$  (which has a decay rate of 0.5 after 50% of iterations)
  - $L_1b$  regularization = 0.025
  - Number of MC step between each update = 5

For the local RBMs trained respectively on the three specificity classes of WW sequences predicted by the original RBM, we use  $M = 30$  and keep all the other hyper-parameters unchanged.

## 4 Statistic of paths sampled in LP

Here we show the relation between the sequences sampled using the sampling procedure described above (using the RBM as model) with the mean-field solution described in the main paper. Looking at Figure S1 We see, consistently with the mean-field solution, that global solutions prefers to activate input 14 more than the direct solution. Furthermore, statistically this input is more likely to be reduced before activating input 4, which is consistent with the mean-field solution.

Analysing the difference between the direct and global paths along each inputs we notice that global solutions maintain high scores in terms of  $p_{nat}$  by exploiting the interactions between amino-acids at sites 5,6,11 and 22 (see Figure 2 in the main paper). Global paths are divided in two classes corresponding to the chemical nature of the interaction used to bind these amino-acids. One cluster (shown in maroon in Figure 2 of the main paper and in Figure S1) uses Cys-Cys bridges to establish this interactions. Instead the most populated cluster (shown in red in the same figures) exploits electrostatic interactions that are not initially present in the target sequences (hence forbidden along direct paths). Some of these interactions are shown in Figure S2. This explains why the Principal Component Analysis shown in Figure 2 of the main paper does not discriminate between direct paths and most of the global ones (*i.e.* red cluster).

To deeper characterize the behaviour of global solutions, we also plot in Figure S3 the average distance from the direct space as a function of time obtained from the paths sampled using  $P_{model} \propto P_{RBM}$ , the likelihood from the trained RBM model.

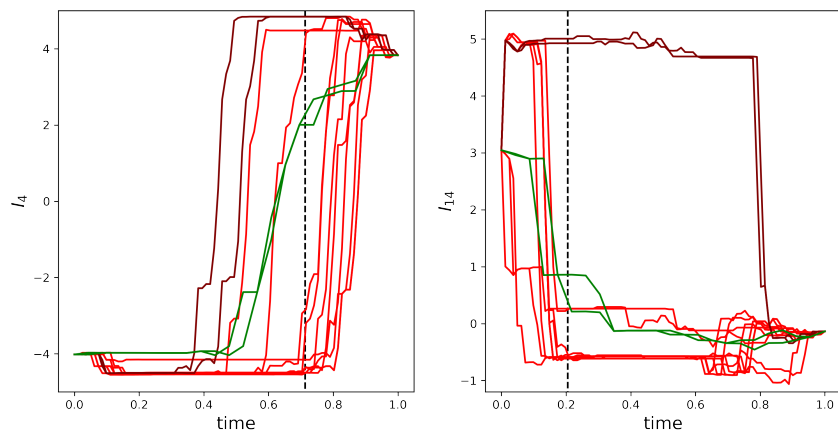


Figure S1: Plot of some relevant inputs as function of time sampled with our Monte-Carlo procedure ( $\Lambda = 2$  and target  $\beta = 3$ ). The colors respect those presented in Figure 2 in the main paper. Black lines correspond to the average time at which the input switch value ( $>0$  for  $I_4$  and  $<2$  for  $I_{14}$ ).

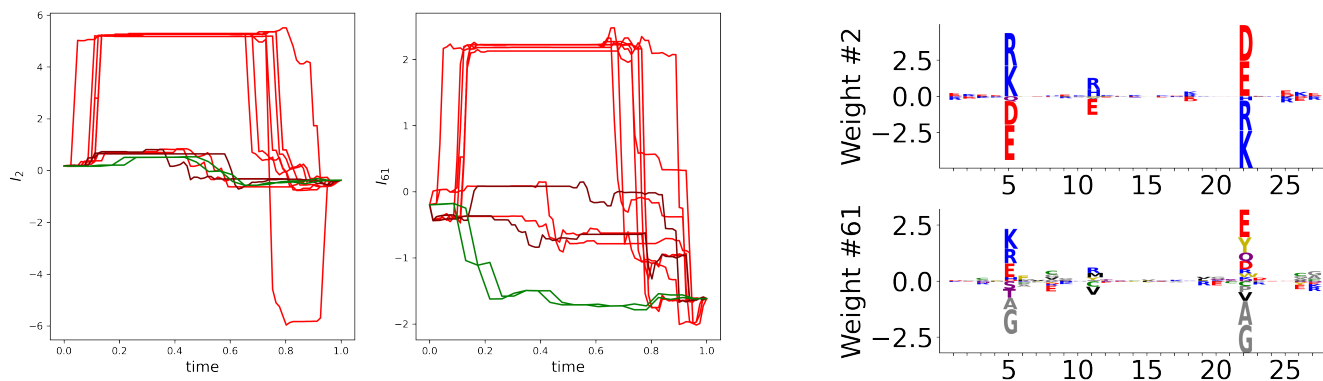


Figure S2: Plot of some relevant inputs (and their respective weights logos) as function of time sampled with our Monte-Carlo procedure ( $\Lambda = 2$  and target  $\beta = 3$ ) exploiting relevant electrostatic interactions forbidden in the direct space. The colors respect those presented in Figure 2 in the main paper.

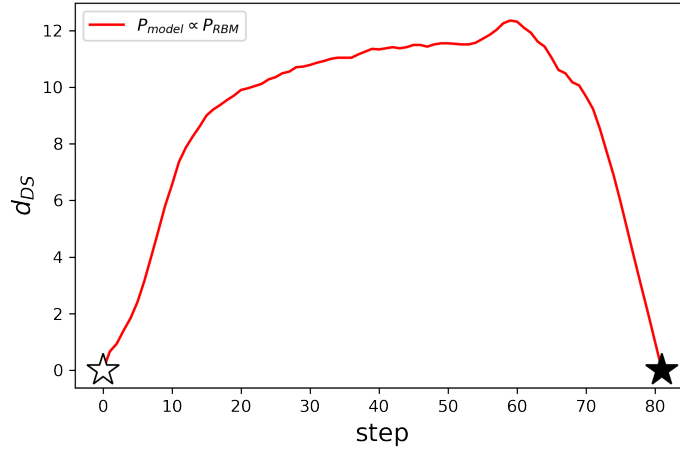


Figure S3: Average value of the distance from direct space (defined as  $d_{DS}(\mathbf{v}) = \sum_i (1 - \delta_{v_i^{start}, v_i})(1 - \delta_{v_i^{end}, v_i})$ ) as a function of the step along the path connecting the two modes in the LP landscape. Black and White stars refer to the same sequences as in Figure 2 of the main text.

## 5 Additional information about mutational paths of the WW domain

### 5.1 Lists of the tested sequences

Here we present the reference sequences sampled with the MC algorithm and tested using AlphaFold (note that the first sequence of each list represent the YAP1 wild-type sequence from [ES99], while the last is the natural wild-type specific for each class) together with the predicted specificity using local RBMs:

- From YAP1 to wild-type of class II:
  - LPAGWEMAKTSS-GQRYFLNHIDQTTWQDP
  - LPAGWEMAKTSD-GERYFINHNTKTTWQDP predicted I
  - LPPGWEEARTPD-GRVYFINHNTKTTWQDP predicted I
  - LPPGWEEARAPD-GRTYYYNHNTKTTWEKP predicted II/III
  - LPPGWTEHKAPD-GRTYYYNHNTKTSTWEKP predicted II/III
  - LPSGWTEHKAPD-GRTYYYNTEKQSTWEKP predicted II/III
  - AKSMWTEHKSPD-GRTYYYNTEKQSTWEKP
- From YAP1 to wild-type of class IV:
  - LPAGWEMAKTSS-GQRYFLNHIDQTTWQDP
  - LPAGWEMRRTPS-GRVYFVNHITRTTQWEDP predicted I
  - LPPGWEERRDPS-GRVYYVNHITRTTQWERP predicted I
  - LPPGWEERSRS-GRVYYVNHITRTTQWERP predicted I
  - LPPGWEKRMSRS-GRVYYVNHITRTTQWERP predicted I
  - LPPGWEKRMSRSSGRVYYVNHITRASQWERP predicted IV
  - LPPGWEKRMSRSSGRVYYFNHITNASQWERP
- From YAP1 to wild-type of class I:
  - LPAGWEMAKTSS-GQRYFLNHIDQTTWQDP
  - LPAGWEMAKTSE-GQRYFINHNTQTTWQDP

- LPPGWEMAYTPE-GERYFINHNTKTTTWLDP
- LPPGWEMGITRG-GRVFFINHETKSTTWLDP
- LPRSWTYGITRG-GRVFFINHEAKSTTWLHP
- LPRSWTYGITRG-GRVFFINEEAKSTTWLHP

## 5.2 details on the TM-score

To compare the inferred structures of the sampled sequences along the path with those of the target natural sequences we used the Template Modelling (TM) score developed in [ZS04] and represents a variation of the Levitt–Gerstein (LG) score [LG98]. Compared to other similarity score (like root-mean-square deviation (RMSD)) it gives a more accurate measure since it relies more on the global similarity of the full sequence rather than the local similarities.

Practically, we consider a target sequence of length  $L_{\text{target}}$  and a template one whose structure has to be compared with. First, we align the two sequences and we take the  $L_{\text{common}}$  pairs of residues that commonly appear aligned. Then the score is computed as

$$\text{TM-score} = \max_{\{d_i\}} \left[ \frac{1}{L_{\text{target}}} \sum_{i=1}^{L_{\text{common}}} \frac{1}{1 + \left( \frac{d_i}{d_0(L_{\text{target}})} \right)^2} \right], \quad (8)$$

where  $d_i$  is the distance between the  $i$ th pair of residues between the template and the target structures after alignment, and  $d_0(L_{\text{target}}) = 1.24(L_{\text{target}} - 15)^{1/3} - 1.8$  is a distance scale that normalizes distances. This formula gives a score between 0 and 1. if  $\text{TM-score} < 0.2$ , the two sequences are totally uncorrelated, while they can be considered to have the same structure if  $\text{TM-score} > 0.5$ . In Figure S4 we show the tables of the TM-scores associated with the sequences tested above.

	YAP1	wt class I		YAP1	wt class IV		YAP1	wt class II
YAP1	1	0.88	YAP1	1	0.76	YAP1	1	0.76
1	0.95	0.83	1	0.93	0.76	1	0.92	0.72
2	0.94	0.86	2	0.9	0.8	2	0.93	0.75
3	0.91	0.82	3	0.89	0.84	3	0.86	0.85
4	0.84	0.98	4	0.81	0.7	4	0.84	0.84
wt class I	0.88	1	5	0.83	0.93	5	0.86	0.83
			wt class IV	0.76	1	wt class II	0.76	1

Figure S4: Table of the TM-scores measured between the structures inferred from AlphaFold.

## 5.3 ProteinMPNN score

The ProteinMPNN model published in [DAB<sup>+</sup>22] takes a reference backbone structure (uploaded as a .pdb file) and gives as output a log-probability function over protein sequences  $\log P_{\text{MPNN}}(\mathbf{v})$  measuring the affinity of the sequence  $\mathbf{v}$  to fold into a specific structure and/or complex. In order to compare values from different models we re-normalised the log-score as

$$\text{norm. score}(\mathbf{v}) = \frac{\log P_{\text{MPNN}}(\mathbf{v}) - \log P_{\text{MPNN}}(\mathbf{v}_{wt1})}{\log P_{\text{MPNN}}(\mathbf{v}_{wt0}) - \log P_{\text{MPNN}}(\mathbf{v}_{wt1})}, \quad (9)$$

where  $\mathbf{v}_{wt0}$  is one of the edge sequences of the path equal to the reference wild-type of the target structure, while  $\mathbf{v}_{wt1}$  is the other edge sequence with different specificity.

Since the transition from class I to class IV requires an insertion along the path (see section 5.1), we decided to remove those insertion to test the sequences against the class I reference backbone structure (PDB ID: 2LTW) and to substitute the gap with Serine (S) to test them against class IV reference structure (PDB ID: 1I8G).

## 6 Derivation of mean-field equations for path sampling with a RBM model

To exploit the nature of the RBM as a mean-field model we rewrite the probability distribution of the model as

$$P_{RBM}(\mathbf{v}) = \frac{1}{Z_{RBM}} \int \prod_{\mu} dh_{\mu} \exp \left( \sum_i g_i(v_i) + \sum_{i,\mu} w_{i\mu}(v_i) h_{\mu} - \sum_{\mu} \mathcal{U}_{\mu}(h_{\mu}) \right) \quad (10)$$

$$= \frac{1}{Z_{RBM}} \exp \left( \sum_i g_i(v_i) + N \sum_{\mu} \Gamma_{\mu} \left( \frac{1}{N} I_{\mu} \right) \right), \quad (11)$$

where  $\gamma$  is defined in the main text.

By introducing the order parameters  $m_t^{\mu} = I_{\mu,t}/N$ ,  $q_t = \frac{1}{N} \sum_i \delta_{v_{i,t}, v_{i,t+1}}$  as well as the overlap potential  $\Phi$ , we can write the probability for a path in the order parameter space as (in the large  $N$  limit)

$$P_{path}(\{\mathbf{m}_t, q_t\}_{t=1}^T; \beta) \propto \sum_{\{\mathbf{v}_t\}} \prod_{t,\mu} \delta \left( \frac{1}{N} \sum_i w_{i\mu}(v_{i,t}) - m_t^{\mu} \right) \prod_t \delta \left( \frac{1}{N} \sum_i \delta_{v_{i,t}, v_{i,t+1}} - q_t \right) P_{RBM}^{\beta}(\mathbf{v}_t) \pi^{\beta}(\mathbf{v}_t, \mathbf{v}_{t+1}) \quad (12)$$

$$= \exp \left[ \beta N \left( \sum_{t,\mu} \Gamma(m_t^{\mu}) - \sum_t \Phi(q_t) \right) \right] \times \quad (13)$$

$$\times \int \left( \prod_{\mu,t} d\hat{m}_t^{\mu} \prod_t d\hat{q}_t \right) \sum_{\{\mathbf{v}_t\}} \exp \left[ \sum_{i,t} g_i(v_{i,t}) + N \sum_{t,\mu} \hat{m}_t^{\mu} \left( \frac{1}{N} \sum_i w_{i\mu}(v_{i,t}) - m_t^{\mu} \right) + N \sum_t \hat{q}_t \left( \frac{1}{N} \sum_i \delta_{v_{i,t}, v_{i,t+1}} - q_t \right) \right] \quad (14)$$

$$\approx \exp \left[ \beta N \left( \sum_{t,\mu} \Gamma(m_t^{\mu}) - \sum_t \Phi(q_t) \right) + N \mathcal{S}(\{\mathbf{m}_t, q_t\}_{t=1}^T) \right] = \exp(-N\beta f_{path}(\{\mathbf{m}_t, q_t\})), \quad (15)$$

where

$$\mathcal{S}(\{\mathbf{m}_t, q_t\}_{t=1}^T) = \min_{\{\hat{\mathbf{m}}_t, \hat{q}_t\}} \frac{1}{N} \sum_i \log Z_i(\{\hat{\mathbf{m}}_t, \hat{q}_t\}) - \sum_{t,\mu} m_t^{\mu} \hat{m}_t^{\mu} - \sum_t q_t \hat{q}_t \quad (16)$$

and

$$Z_i(\{\hat{\mathbf{m}}_t, \hat{q}_t\}) = \sum_{v_1, \dots, v_t, \dots, v_T} \exp \left[ \sum_t g_i(v_t) + \sum_{t,\mu} \hat{m}_t^{\mu} w_{i\mu}(v_t) + \sum_t \hat{q}_t \delta_{v_t, v_{t+1}} \right]. \quad (17)$$

Under minimization we find the result shown in the main paper. To obtain numerically the set of magnetizations and overlap that minimize the free energy, we note that the saddle point equation for  $f_{path}$  leads to the following self-consistent equation:

$$m_t^{\mu} = \frac{1}{N} \sum_i \frac{1}{Z_i} \sum_{v_1, \dots, v_t, \dots, v_T} w_{i\mu}(v_t) \exp \left[ \sum_t g_i(v_t) + \sum_{t,\mu} \hat{m}_t^{\mu} w_{i\mu}(v_t) + \sum_t \hat{q}_t \delta_{v_t, v_{t+1}} \right] \quad (18)$$

$$q_t = \frac{1}{N} \sum_i \frac{1}{Z_i} \sum_{v_1, \dots, v_t, \dots, v_T} \delta_{v_t, v_{t+1}} \exp \left[ \sum_t g_i(v_t) + \sum_{t,\mu} \hat{m}_t^{\mu} w_{i\mu}(v_t) + \sum_t \hat{q}_t \delta_{v_t, v_{t+1}} \right], \quad (19)$$

where  $\hat{q}_t = -\beta \Phi'(q_t)$  and  $\hat{m}_t^{\mu} = \beta \Gamma'_{\mu}(m_t^{\mu})$ . We solve this set of equations using gradient descent. To compute the LHS we first compute the partition functions  $Z_i$  using the transfer matrix method and then we take their gradient using automatic differentiation technique built in the Python library JAX [BFH<sup>+</sup>18].

### 6.1 Consensus sequence from MF solutions and the case for WW domain

To obtain the average distance from the direct space, we need to compute at each time at each site the probability of a specific state  $a = 1, \dots, A$ . This can be computed as

$$f_{i,t}(a|\{\mathbf{m}_t, q_t\}) = \frac{\partial}{\partial g_{it}(a)} \log Z_{path} = \frac{\partial}{\partial g_{it}(a)} \sum_{\mathcal{V}} \exp \left[ \sum_{i,t,a} g_{it}(a) \delta_{a,v_{it}} + N \sum_{\mu,t} \Gamma(m_{\mu}^t) - N \sum_t \Phi(q_t) \right] = \frac{\partial}{\partial g_{it}(a)} \log Z_i, \quad (20)$$

where we write  $g_{it}(a) = g_i(a)$  for any  $t$ . Once  $f_{i,t}$  is computed, we obtain the consensus sequence  $\mathbf{v}_t = \{v_{i,t} = \operatorname{argmax}_a f_{i,t}\}$ . The consensus sequences for the MF path shown in Figure (4) of the main paper are:

- I→IV Cont scenario:

- LPAGWEMAKTSS-GQRYFLNHITRTTWQDP
- LPAGWEMRKTSS-GQVYFLNHITRTTWEDP
- LPPGWEMRKTSS-GRVYFLNHITRTTQWEDP
- LPPGWEMRKSRS-GRVYFLNHITRTTQWEDP
- LPPGWEKRKSRS-GRVYYLNHITRTTQWERP
- LPPGWEKRMSRS-GRVYYLNHITRTTQWERP
- LPPGWEKRMSRS-GRVYYFNHITRASQWERP

- I→IV Evo scenario:

- LPPGWEKRKSRS-GRVYYLNHITKTTQWERP
- LPPGWEKRKSRS-GRVYYLNHITKTTQWERP
- LPPGWEKRKSRS-GRVYYLNHITKTTQWERP
- LPPGWEKRKSRS-GRVYYLNHITKTTQWERP
- LPPGWEKRKSRS-GRVYYLNHITKTTQWERP
- LPPGWEKRMSRS-GRVYYLNHITKTTQWERP
- LPPGWEKRMSRS-GRVYYLNHITKTTQWERP

- I→II Cont scenario:

- LPAGWEMAKTSD-GQRYFLNHITQTTTWQDP
- LPAGWEMAKTPD-GQRYFLNHITKTTTWEDP
- LPAGWEEAKTPD-GRTYFYNHITKTTTWEDP
- LPAGWEEAKTPD-GRTYYYNHITKTTTWEKP
- LPAGWTEHKTPD-GRTYYYNHITKTTTWEKP
- LPSGWTEHKTPD-GRTYYYNTITKQSTWEKP
- LPSGWTEHKSPD-GRTYYYNTETKQSTWEKP

- I→II Evo scenario:

- LPAGWEEAKTPD-GRRYFLNHITKTTTWEDP
- LPAGWEEAKTPD-GRTYYYNHITKTTTWEDP
- LPAGWEEAKTPD-GRTYYYNHITKTTTWEKP
- LPAGWEEAKTPD-GRTYYYNHITKTTTWEKP
- LPSGWTEHKTPD-GRTYYYNTITKQSTWEKP
- LPSGWTEHKTPD-GRTYYYNTETKQSTWEKP
- LPSGWTEHKSPD-GRTYYYNTETKQSTWEKP

## 6.2 Free energy optimisation in mean-field theory

In order to obtain the minimum of the free energy in the mean-field approximation we first modify the energetic term of the RBM model by multiplying it with temperature factor  $\beta_0$  (the interaction term  $\sum_t \Phi(q_t)$  stays untouched). Starting from  $\beta_0 = 0$ , we minimize the free-energy using gradient descent. Here the landscape is convex and the gradient descent finds the global minima. Using this solution as a new initial configuration, we re-use gradient descent but after having increased  $\beta_0$  by a small step  $\delta\beta_0$ . In such a way we can follow the global minimum (under the hypothesis that the system does not encounter zeroth-order phase transitions). Then we repeat this procedure until we reach  $\beta_0 = 1$ .

## 7 Neutral theory of evolution

Let's consider a sequence (with  $A$  number of states per site) evolving under mutations only. Given a site  $i$  along the sequence the probability of that site to be in a given state  $A$  at time  $t$ ,  $x_a^i(t)$ , evolve through time under the following equation:

$$\frac{d}{dt}x_a^i(t) = -\mu x_a^i(t) + \frac{\mu}{A} \sum_{b \neq a} x_b^i(t) = \sum_b W_{a,b} x_b^i(t) \quad (21)$$

where  $\mu$  is the mutation rate. Solving the linear differential equation, we can compute the probability that a site mutate into a specific new state in the time interval  $\Delta t$  as

$$p_{\neq} = \frac{1}{A} \left( 1 - e^{-\frac{A\mu\Delta t}{1-A}} \right), \quad (22)$$

while the probability of not mutating is  $p_{=} = 1 - (A-1)p_{\neq}$ . Here we set  $\Delta t = 1$ . Hence the probability of evolving from a sequence  $\mathbf{v}$  to  $\mathbf{v}'$  is

$$\pi(\mathbf{v}, \mathbf{v}') = p_{=}^{Nq} p_{\neq}^{N(1-q)} = e^{-N\Phi(q)}, \quad (23)$$

where  $q$  is the overlap between the two sequence and  $\Phi(q) = q \log \frac{p_{\neq}}{p_{=}} - \log p_{\neq}$ . Hence, the probability to go from  $\mathbf{v}_0$  to  $\mathbf{v}_T$  in  $T$  steps is

$$P(\mathbf{v}_0 \rightarrow \mathbf{v}_T; T) = \sum_{\{\mathbf{v}\}_{t=1}^{T-1}} \pi(\mathbf{v}_0, \mathbf{v}_1) \pi(\mathbf{v}_1, \mathbf{v}_2) \dots \pi(\mathbf{v}_{T-1}, \mathbf{v}_T) = \sum_{\{\mathbf{v}\}_{t=1}^{T-1}} e^{-N \sum_t \Phi(q_t)}, \quad (24)$$

which can be computed exactly as

$$P(\mathbf{v}_0 \rightarrow \mathbf{v}_T; T) = \frac{p_{\neq}^{TN}}{A^N} \left[ \left( \frac{p_{=}}{p_{\neq}} + A - 1 \right)^T - \left( \frac{p_{=}}{p_{\neq}} - 1 \right)^T \right]^D \left[ \left( \frac{p_{=}}{p_{\neq}} + A - 1 \right)^T - (1 - A) \left( \frac{p_{=}}{p_{\neq}} - 1 \right)^T \right]^{N-D}, \quad (25)$$

where  $D$  is the Hamming distance between the two sequences. The last equation correspond to Kimura's theory of neutral evolution [Kim83] and the probability as a maximum for a certain optimal  $T^*$  and converges to  $1/A^N$  for  $T \rightarrow \infty$ .

## References

- [BFH<sup>+</sup>18] James Bradbury, Roy Frostig, Peter Hawkins, Matthew James Johnson, Chris Leary, Dougal Maclaurin, George Necula, Adam Paszke, Jake VanderPlas, Skye Wanderman-Milne, and Qiao Zhang. JAX: composable transformations of Python+NumPy programs, 2018. Available online at: <http://github.com/google/jax>.
- [DAB<sup>+</sup>22] Justas Dauparas, Ivan Anishchenko, Nathaniel Bennett, Hua Bai, Robert J Ragotte, Lukas F Milles, Basile IM Wicky, Alexis Courbet, Rob J de Haas, Neville Bethel, et al. Robust deep learning-based protein sequence design using proteinmpnn. *Science*, page eadd2187, 2022.
- [ES99] Xavier Espanel and Marius Sudol. A single point mutation in a group i ww domain shifts its specificity to that of group ii ww domains. *Journal of Biological Chemistry*, 274(24):17284–17289, 1999.
- [FI12] Asja Fischer and Christian Igel. An Introduction to Restricted Boltzmann Machines. In *Progress in Pattern Recognition, Image Analysis, Computer Vision, and Applications*, pages 14–36. Springer, Berlin, Germany, September 2012.

- [JGS<sup>+</sup>16] Hugo Jacquin, Amy Gilson, Eugene Shakhnovich, Simona Cocco, and Rémi Monasson. Benchmarking inverse statistical approaches for protein structure and design with exactly solvable models. *PLOS Computational Biology*, 12(5):1–18, 05 2016.
- [Kim83] Motoo Kimura. *The neutral theory of molecular evolution*. Cambridge University Press, 1983.
- [LD89] Kit Fun Lau and Ken A. Dill. A lattice statistical mechanics model of the conformational and sequence spaces of proteins. *Macromolecules*, 22(10):3986–3997, October 1989.
- [LG98] Michael Levitt and Mark Gerstein. A unified statistical framework for sequence comparison and structure comparison. *Proceedings of the National Academy of sciences*, 95(11):5913–5920, 1998.
- [MJ96] Sanzo Miyazawa and Robert L. Jernigan. Residue – Residue Potentials with a Favorable Contact Pair Term and an Unfavorable High Packing Density Term, for Simulation and Threading. *J. Mol. Biol.*, 256(3):623–644, March 1996.
- [TCM19] Jérôme Tubiana, Simona Cocco, and Rémi Monasson. Learning protein constitutive motifs from sequence data. *eLife*, 8:e39397, March 2019.
- [Tie08] Tijmen Tieleman. Training restricted Boltzmann machines using approximations to the likelihood gradient. In *ICML '08: Proceedings of the 25th international conference on Machine learning*, pages 1064–1071. Association for Computing Machinery, New York, NY, USA, July 2008.
- [Tub18a] Jérôme Tubiana. *Restricted Boltzmann machines : from compositional representations to protein sequence analysis*. PhD thesis, Université Paris sciences et lettres, Paris, France, November 2018.
- [Tub18b] Jerome Tubiana. Probabilistic graphical models (pgm), 2018. Available online at: <https://github.com/jertubiana/PGM>.
- [ZS04] Yang Zhang and Jeffrey Skolnick. Scoring function for automated assessment of protein structure template quality. *Proteins: Structure, Function, and Bioinformatics*, 57(4):702–710, 2004.